Dalton Transactions

ROYAL SOCIETY OF CHEMISTRY

PAPER

View Article Online
View Journal | View Issue

Cite this: *Dalton Trans.*, 2021, **50**, 10436

Highly uniform self-assembled monolayers of silver nanospheres for the sensitive and quantitative detection of glutathione by SERS†

Cailing Jiang,[a] Feixiang Huang,*[b] Yi Chen *[a] and Li Jiang [a]

Received 6th May 2021,
Accepted 23rd June 2021

DOI: 10.1039/d1dt01474a

rsc.li/dalton

The homeostasis and imbalance of glutathione (GSH), an important antioxidant in organisms, are one of the key signals that reflect the health of organisms. In this paper, a novel SERS sensing platform based on Ag film@Si that self-assembled using silver nanospheres was proposed, which was used for the highly sensitive and selective detection of GSH. With the aid of an oil/water/oil three-phase system, the nano-silver film was self-assembled and finally deposited on silicon wafers. The heterobifunctional crosslinking agent *N*-succinimidyl-3-(2-pyridyldithio)propionate (SPDP), which contains pyridine rings and disulfide bonds, was involved in the exchange reaction between the sulfhydryl groups and disulfide bonds. With the addition of GSH, the breakage of disulfide bonds was promoted, thereby enhancing the SERS signal of SPDP. GSH can be detected sensitively by detecting the changes in the SPDP signal. The detection limit of GSH is 10 nM, and the method is still highly stable when the external environment is serum or other more complex environments.

Introduction

Glutathione is a low-molecular-weight thiol tripeptide, divided into oxidized (GSSG) and reduced (GSH) forms.[1–3] Most glutathione in cells is in the reduced form (>95%), and the normal concentration ranges from 0.5 to 10 mM.[2] As an important antioxidant *in vivo*, it participates in many metabolic processes and its homeostasis and imbalance have attracted widespread attention.[4] Reactive oxygen species are products of normal metabolism in the body. During the period of metabolism and immune response, the level of glutathione will increase as the level of reactive oxygen species increases. The dynamic balance between the two supports the adjustment of the redox system and signal transmission.[4–6] Compared to the normal breast tissue, the level of glutathione in breast tumors is significantly higher.[7] But some diseases also seem to be worsened by lower glutathione levels.[4] Mitochondria, for example, are important sources of reactive oxygen species, and damage to mitochondrial function is usually related to glutathione depletion.[4,8,9] In addition, glutathione levels are also significantly reduced in esophagus, stomach and liver tumors.[7] Another function of glutathione that cannot be ignored is the detoxification of exogenous and endogenous compounds.[2] At present, the global COVID-19 epidemic situation is still grim. Alexey Polonikov *et al.* have shown that with aging, endogenous glutathione deficiency may be an important reason for the severe symptoms and even death of COVID-19 patients.[2,10] Therefore, detecting the changes in the serum glutathione level is of great significance for early diagnosis of the disease.

The active group of glutathione is sulfhydryl (–SH), and the standard method for detecting the sulfhydryl group is with the aid of the sulfhydryl reagent DTNB, which yields 2-nitro-5-thiobenzoate (TNB^{2-}) through thiol–disulfide bond exchange with GSH. The absorbance was measured at 412 nm to indirectly realize the quantitative determination of GSH.[11] In addition, varieties of methods for detecting glutathione have been proposed in recent years, like fluorometry,[12–15] high performance liquid chromatography (HPLC),[16,17] electrochemical analysis[18,19] or colorimetry.[20–22] However, there are disadvantages such as high cost and complicated experiment procedures. It is still worthwhile to develop low-cost, fast, and efficient methods.

With the unique optical properties of metal nanoparticles, combined with the molecular fingerprint information provided by Raman spectroscopy, the surface-enhanced Raman spectroscopy (SERS) technology has attracted widespread attention in the field of biomolecular detection.[11,23,24] SERS utilizes the isoplasmon effect of metals[25] (gold, silver, copper, *etc.*) to adsorb specific Raman signal molecules on or near their surfaces to enhance the standard Raman intensity of the molecules, and the enhancement effect is more significant in the hot spots formed by the adjacent metal nanojunction or its

[a]*College of Optical and Electronic Technology, China Jiliang University, Hangzhou 310018, P. R. China. E-mail: chenyi@cjlu.edu.cn*
[b]*Department of TCM Gynecology, Hangzhou Women's Hospital, Hangzhou 310018, P. R. China. E-mail: fxhuang2009@163.com*

†Electronic supplementary information (ESI) available. See DOI: 10.1039/d1dt01474a

edges.[26–28] As an ultra-sensitive vibration spectrum technology, the two main advantages of SERS are that the signal is very strong and can realize the detection of a single molecule, followed by great specificity.[29] On the whole, the application of SERS can be divided into two categories: labeled and label-free detection.[30] Kuligowski *et al.* developed a label-free method for detecting glutathione in whole blood using AgNPs as the SERS substrate. The relationship between the GSH concentration and SERS signal was established by combining SERS and chromatography, the sensitivity reached the limit when the concentration of glutathione was 13 μM.[31] In order to improve the measurement accuracy, the research team combined isotope labeling (IS) and SERS to realize the direct quantification of GSH.[24] Compared to label-free detection, the use of isotope labeling for labeled detection improved the selectivity and repeatability of SERS detection, whereas the cost was relatively high and label processing was relatively complex. It is well known that GSH, as a part of the cysteine residue, has a small Raman cross section and a low Raman response. Detecting glutathione without labeling is very difficult. Therefore, more researchers have turned to labeled detection. Wang *et al.* reported a SERS probe of 4-MP functionalized gold flowers. When detecting ClO^-, the SERS spectrum would change and then GSH was added and the SERS spectrum would recover the SERS spectrum of the original substrate, so as to realize the simultaneous determination of ClO^- and GSH.[32] This method realized the high-precision ratio detection of the two, but the seed growth method was relatively strict. Based on the thiol–disulfide bond exchange reaction, Wei *et al.* designed a PDEA-modified AgNPs@Si substrate to achieve the specific detection of glutathione.[11] However, there is still room for improvement in the synthesis of complex reagents.

The convenience and versatility of the self-assembled SERS substrate have attracted many researchers to devote themselves to its research and development,[33,34] especially the high portability of the liquid–liquid interface self-assembled SERS substrate. Silver nanoparticles of various shapes including nanospheres, nanowires, nanorods, nanoflowers and so on are widely used in the SERS sensor platform. In this paper, a new type of Ag film@Si SERS substrate was designed and *N*-succinimidyl-3-(2-pyridyldithio)propionate (SPDP) was used as the Raman reporter to achieve the highly consistent and highly sensitive detection of GSH. Considering the perfect geometric symmetry of spherical nanoparticles[35] and the local electromagnetic field formed by the seamless contact between the edges of adjacent particles, spherical silver nanoparticles can generate rich hot spots, enhance the SERS signal of target detection objects and improve the sensitivity. The self-assembled spherical silver nanoparticles form a dense silver film on the silicon wafer to form an SERS platform for solid phase detection, which improves the uniformity and repeatability, with low cost, simple synthesis, and portability. SPDP is a heterobifunctional crosslinking agent with a pyridine disulfide group. The addition of glutathione promoted the breaking of the disulfide bond, thereby enhancing the SERS signal of SPDP. The SERS sensor platform constructed in this paper realized the quantitative and selective detection of glutathione. It has the advantages of being quick and clear, simple to prepare and environmentally friendly, which has provided a basis for practical application.

Experimental section

Chemicals and materials

Silicon (111) wafer (boron-doped) was bought from Kaihua Shunchen Electronic Technology Co., Ltd. Ascorbic acid (AA), trisodium citrate, citric acid and polyvinylpyrrolidone (PVP) were purchased from Yuanye Biological Technology Co., Ltd (Shanghai, China). Sodium hydroxide (NaOH), dichloromethane (CH_2Cl_2) and *n*-hexane were purchased from Macklin Biochemical Technology Co., Ltd (Shanghai, China). Silver nitrate ($AgNO_3$) was purchased from Xiya Reagent. DMSO, *N*-succinimidyl-3-(2-pyridyldithio)propionate (SPDP), L-homocysteine were purchased from Aladdin Biochemical Technology Co., Ltd (Shanghai, China). Glutathione, glutamic acid, D-glucose anhydrous, L-cysteine, L-histidine, L-lysine, and L-glycine were purchased from Bomeibio (Hefei, China). Phosphate buffered saline was purchased from TransGen Biotech. All reagents were used without further purification. High-purity water (18.2 MΩ cm) was used in all the experiments.

Synthesis and self-assembly of Ag film@Si

Silver nanoparticles were synthesized through the reduction method referring to the literature,[36] where $AgNO_3$ was typically reduced by ascorbic acid. Concretely, 40 mL of aqueous solution containing ascorbic acid (0.6 mM) and trisodium citrate (3 mM) was prepared and adjusted to different pH values (6.0, 7.0, 8.0, 9.0, 10.0, or 10.5) by adding 0.2 M citrate acid or 0.1 M NaOH solution. 0.1 M $AgNO_3$ solution (0.4 mL) was injected into the mixed solution under a stirring speed of 900 rpm in a 30 °C oil bath. The reaction solutions were observed to change from colorless to yellow and then brown (at pH 10.5) or blue turbid (at pH 6.0, 7.0, 8.0, 9.0 and 10.0). After 15 min, no further change occurred, indicating that the reaction was complete. Then, it was heated at 80 °C for 2 hours to promote intraparticle maturation. A condenser was used to prevent the evaporation of the solvent. After being heated over and down to room temperature, the silver nanoparticles were transferred to a 50 mL centrifuge tube and stored (4 °C) for future assembly applications.

Ag NP monolayer films were prepared according to the method reported by Lin *et al.*[37] Firstly, 6 mL of nanoparticle solution was mixed with 9 mL of ultrapure water. After centrifugation at 7500 rpm for 20 min, the precipitates were collected and dispersed into 1 mL of PVP ethanol solution (1 wt%, 5.5 W). Then, it was shaken vigorously and allowed to stay overnight. After centrifugation, the PVP-coated Ag NPs were obtained and redispersed in 1 mL of ethanol. To assemble the PVP-coated Ag NPs, 400 μL of PVP stabilized nanoparticle solution and 800 μL of dichloromethane were mixed with 2 mL of water in a 5 mL centrifuge tube. After shaking

thoroughly and allowing to stand for a while, the centrifuge tube was slightly tilted and then 800 μL of *n*-hexane was added slowly. A silver nanofilm was then formed at the interface between *n*-hexane and water. Then, *n*-hexane was slowly extracted and the nanofilm was transferred onto the hydrophilic silicon wafers.

Instruments

The UV-vis absorption spectra of a 1 : 10 dilution of the silver nanoparticles with high-purity water were recorded using a UV spectrometer (TU-1901, PERSEE, Beijing). The morphological features of the Ag NP monolayer film were detected by a field-emission scanning electron microscope (SEM, Hitachi SU-8010). The Raman spectra were recorded by a confocal micro-Raman spectrometer (Horiba LabRAM Evolution 800) at a wavelength of 532 nm using a solid state laser. A microplate reader (FlexA-200, ALLSHENG, Hangzhou) was used to dynamically measure the absorbance.

Surface enhanced Raman spectroscopy measurement

The standard stock solution of GSH (0.1 mM) was prepared by dissolving 0.307 mg of GSH solids in 10 mL of PBS. Then, it was gradually diluted to the required series of concentrations with the same solvent and stored at 4 °C for further use. In order to obtain the linear dynamic range and detection limit of the detection method, a gradient concentration of GSH was prepared, including 10 nM, 25 nM, 50 nM, 100 nM, 500 nM, 1 μM and 2 μM. 0.1 mM SPDP was prepared by weighing SPDP solids and dissolving them in 10 mL of DMSO. In order to make the silver film fully contact the analyte, the silver film was soaked in a centrifuge tube containing 50 μL of SPDP for 2 hours and then taken out for further measurement. 0.1 mM SPDP (50 μL) was incubated with different concentrations of GSH (50 μL) for 2 hours at room temperature. Silver films were soaked in the mixture for 2 hours and then taken out for further measurements. In order to avoid any accidental phenomena in the experiment, the experiment was repeated several times. The selectivity was tested by comparing the SERS signals of GSH and other amino acids with similar chemical structures including glutamic acid, D-glucose anhydrous, L-cysteine, L-histidine, L-lysine, L-glycine and L-homocysteine.[11] A solution of 1 μM of different amino acids was prepared by weighing the corresponding solids and dissolving them in 10 mL of PBS. Each amino acid solution was mixed and incubated with SPDP for two hours, and then SERS measurement was carried out as described above.

Results and discussion

Characterization and evaluation of the Ag film SERS platform

Ag film@Si is used to establish the SERS sensor platform by the self-assembly of the synthesized silver nanoparticles onto silicon wafers. Fig. 1A is an SEM image of colloidal silver nano-

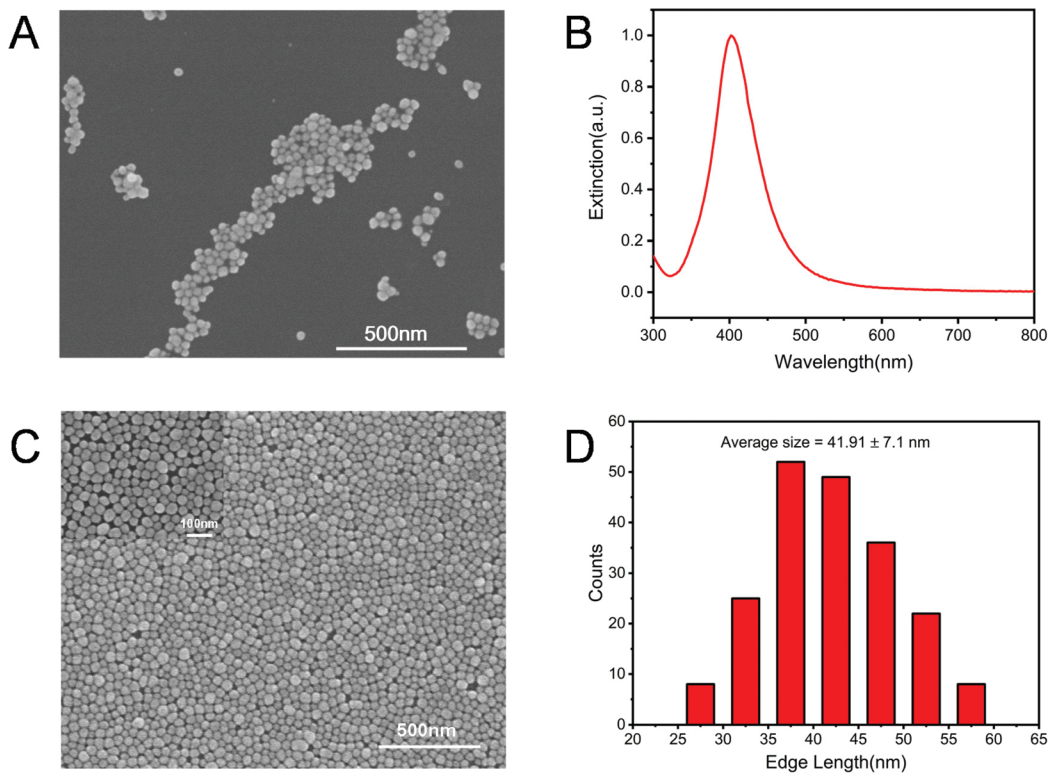

Fig. 1 (A) The SEM image of silver nanoparticles randomly dispersed on a silicon wafer. (B) The ultraviolet–visible absorption spectrum of colloidal silver nanoparticles. (C) The SEM image of the self-assembled Ag film@Si. (D) The histogram of particle size distribution of the monolayer silver film.

particles, the shape of the silver nanoparticles was spherical and the diameter distribution was relatively uniform, about 30–50 nm. The UV-vis absorption spectra of the colloidal silver nanoparticles are shown in Fig. 1B, which indicate that the AgNPs have an absorption peak roughly located at 402 nm and the half-peak width is 62 nm, which indirectly reflects the slight difference in particle size among the nanoparticles. The results are consistent with other studies[38] on the synthesis of silver nanoparticles, indicating that silver nanoparticles were successfully synthesized.

The process of the self-assembly of silver nanoparticles refers to the three-phase oil/water/oil system proposed by Lin *et al.*,[37] which overcomes the shortcomings of uneven substrates due to the irregular aggregation of silver nanoparticles. The specific description is shown in Scheme 1. The PVP-coated Ag NPs, dichloromethane and water were successively added to a 5 mL centrifuge tube. After being shaken thoroughly and left standing, a tight accumulation layer was formed at the oil/water interface composed of dichloromethane/water. The centrifuge tube was properly inclined and another layer of oil-phase *n*-hexane was added. Since water is more dense than *n*-hexane, the Ag NPs spontaneously rise to the water/*n*-hexane interface to form a bright yellow metal film with the help of oil–water interfacial tension. After *n*-hexane was sucked out, the Ag film was loaded onto the silicon wafer. From the SEM image of the Ag film@Si, as shown in Fig. 1C, the distribution of Ag film is uniform. The particle size statistical distribution of the Ag film is shown in Fig. 1D. The average diameter of the Ag NPs is 41.91 ± 7.1 nm and the particle size distribution of the synthesized silver nanoparticles is uniform. In order to evaluate the SERS performance of the Ag film@Si substrate, the SERS signals of SPDP were detected at an excitation wavelength of 532 nm. Fig. 2A shows the Raman signal of solid SPDP (Fig. 2A(a)) and SERS signal enhanced by Ag film@Si (Fig. 2A(b)). The band at 529 cm^{-1} is attributed to the disulfide bond vibrations[39] and the main vibrations at 985, 1046, 1085 and 1116 cm^{-1} are all from the pyridine ring.[11,38] Since SPDP contains disulfide bonds, it will interact with the silver surface.[40–42] The SPDP solution was tested under the same conditions, as shown in Fig. 2A(b), the main vibration at 1000, 1049, 1084 and 1121 cm^{-1} are from the pyridine ring.[11,38] Moreover, the Ag film@Si greatly enhanced the SERS signal of SPDP, which reflects the excellent enhancement performance of the self-assembled SERS sensor platform. The uniformity of the substrate was evaluated by a thermodynamic chart and relative standard deviations of the mapping area. The size of the mapping area was 16 μm × 16 μm, the scanning step was 1 μm. Fig. 2 shows the content of the mapping spectrum of the SPDP molecules at a concentration of 0.1 mM, the intensity heat map (Fig. 2B) and 3D waterfall diagram (Fig. 2C) indicate the high uniformity of the SERS signals. In order to quantitatively assess the uniformity of the SERS signal, the relative standard deviation (RSD) of the intensity at 1551 cm^{-1} in the mapping area was calculated which was 8.41% (Fig. 2D), indicating the uniformity of the Ag film@Si SERS sensor platform in a wide range. Simultaneously, in order to explore the repeatability of the SERS platform, the SERS signals of SPDP on five different batches of Ag film@Si were compared. For

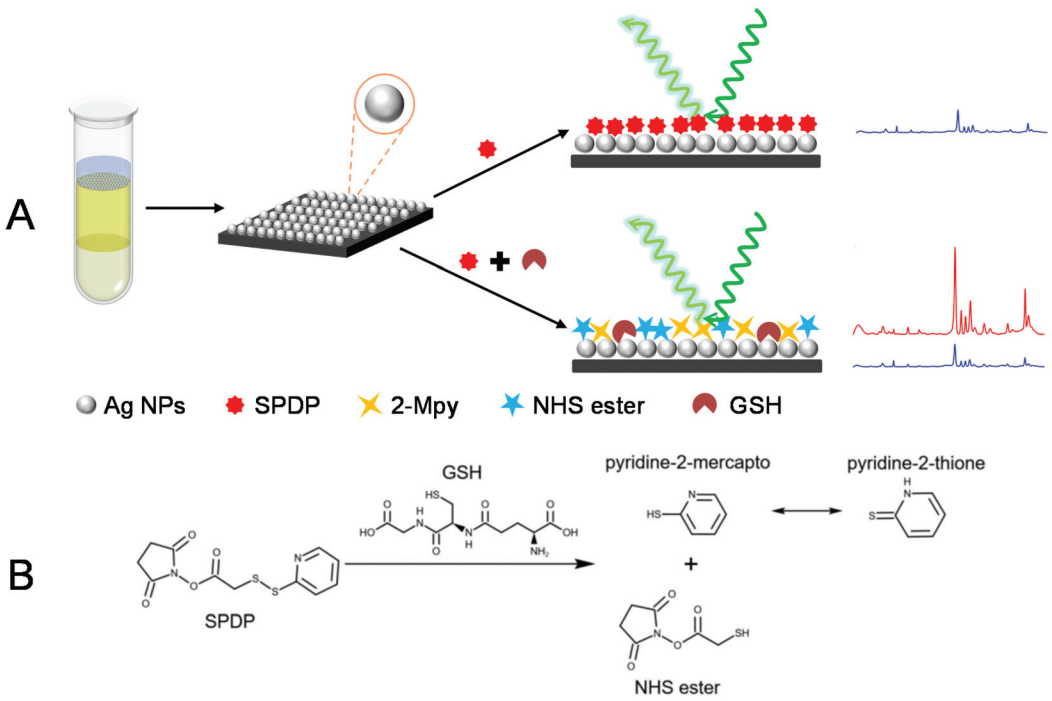

Scheme 1 (A) Schematic diagram of the Ag film@Si SERS platform detecting GSH. (B) The chemical structure diagram of the reaction process of SPDP and GSH.

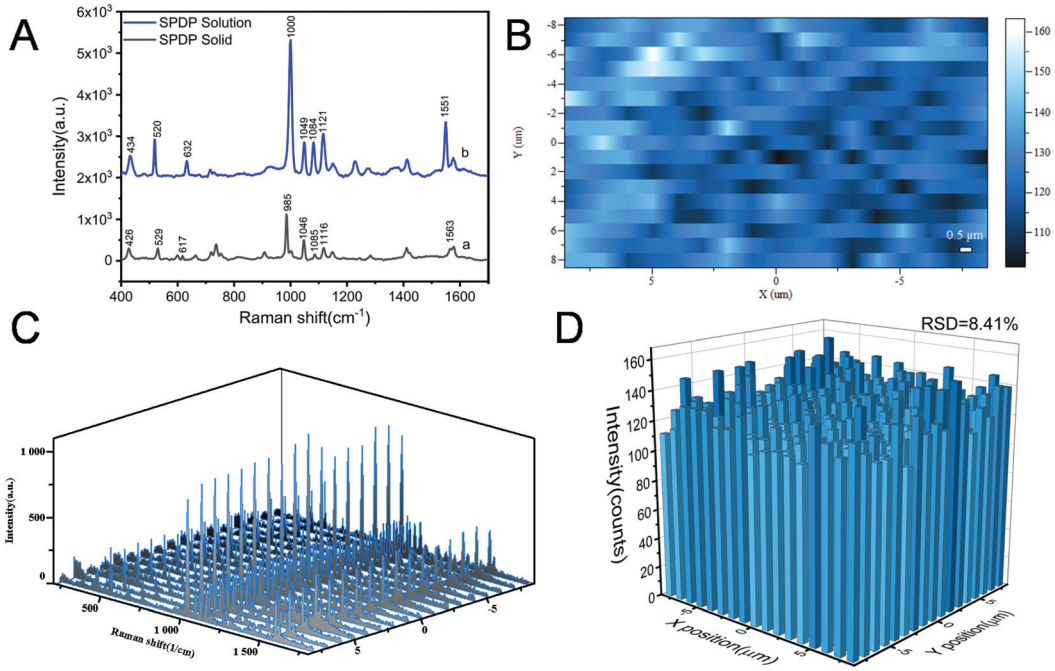

Fig. 2 (A) (a) The Raman spectrum of SPDP powder, (b) the SERS spectrum of 0.1 mM SPDP on Ag film@Si. (B) The intensity heat map of the SERS spectrum of 0.1 mM SPDP; the size of mapping area was 16 μm × 16 μm. (C) The SERS spectrum of SPDP scanned by multiple points on Ag film@Si. (D) The 3D histogram of SERS intensity corresponding to the mapping area.

details, see the ESI (Fig. S1†). The RSD value of 9.64% at 1000 cm^{-1} is calculated quantitatively, indicating that the SERS platform had good repeatability.

SERS detection of glutathione

N-Succinimidyl-3-(2-pyridyldithio)propionate (SPDP) is a heterobifunctional crosslinking agent with amine and sulfhydryl reactivity, which consists of *N*-hydroxysuccinimide ester (NHS) and pyridine disulfide groups and disulfide bonds in its spacer arm. Fig. S2† shows the process of the chemical reaction with the aid of the chemical structure. Fig. S2A† indicates that when the disulfide group of SPDP reacts with thiol, the disulfide bond will be broken. The chemical structure in Scheme 1 shows the reaction process, and a detailed description is also given in the ESI.† Reduced glutathione is one of the reduced thiols, and the exchange reaction of the thiol disulfide bond can promote the breaking of the disulfide bond (Scheme 1B). The pyridine disulfide group of SPDP and the sulfhydryl group of glutathione undergo the exchange reaction of the sulfhydryl disulfide bond to generate the NHS ester with the sulfhydryl group and pyridine-2-mercapto or pyridine-2-thione,[43,44] which will be bound with silver through an Ag–S bond.[45]

Through the research of Kuligowski *et al.*, we have learned that the Raman scattering cross section of glutathione is very small,[24,31] which makes it difficult to carry out label-free detection and has low sensitivity. Therefore, here SPDP is used as the Raman reporter molecule. Scheme 1 shows the procedure of the indirect detection of glutathione with the aid of this molecule. As shown in Fig. 3A, when the concentration of SPDP is increased from 10^{-7} M to 10^{-3} M, the SERS signals are continuously enhanced and they reach saturation when the concentration was higher than 10^{-4} M. Therefore, it was determined to use 0.1 mM SPDP for subsequent experiments. Among them, the SERS spectrum of the solvent DMSO is shown in Fig. 3A(a), with its characteristic Raman peak at 677 cm^{-1}, which is attributed to the C–S stretch vibration.[46] Fig. 3B(b) shows the SERS spectra of 0.1 mM SPDP tested under the same conditions after one month interval. There is little difference in the SERS intensity before and after the comparison, indicating the high stability of the substrate. Fig. 4A compares the SERS intensity of SPDP with or without glutathione. After SPDP was incubated with GSH for two hours, the reduced glutathione with active sulfhydryl groups breaks the disulfide bonds of SPDP. Pyridine-2-mercapto was replaced and combined with the silver nanoparticles through thiol–silver bonds,[42] thus greatly enhancing the SERS signal of SPDP. In order to explore the uniformity of the SERS platform at this time, we set a range of 16 μm × 16 μm for point-by-point scanning to record the mapping spectrum in the presence of 1 μM GSH. Fig. 4B and C, respectively, show the intensity heat map and 3D waterfall map of the mapping area; the RSD of the SERS intensity at 1000 cm^{-1} in this area is found to be 7.65% through quantitative calculation, which comprehensively showed that the existence of GSH did not affect the uniformity of the substrate and further reflected the high uniformity of the substrate.

In order to evaluate the sensitivity of the Ag film@Si SERS platform, a series of prepared concentrations of GSH and

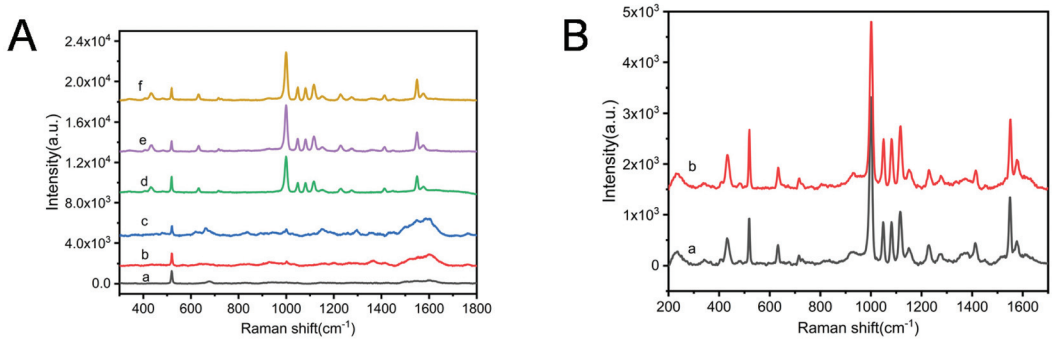

Fig. 3 (A) The SERS spectra of different concentrations of SPDP on Ag film@Si, from a to f are 0 M, 10^{-7} M, 10^{-6} M, 10^{-5} M, 10^{-4} M, and 10^{-3} M. (B) (a) The SERS spectrum of 0.1 mM SPDP on Ag film@Si and (b) the SERS spectrum of (a) after one month of storage.

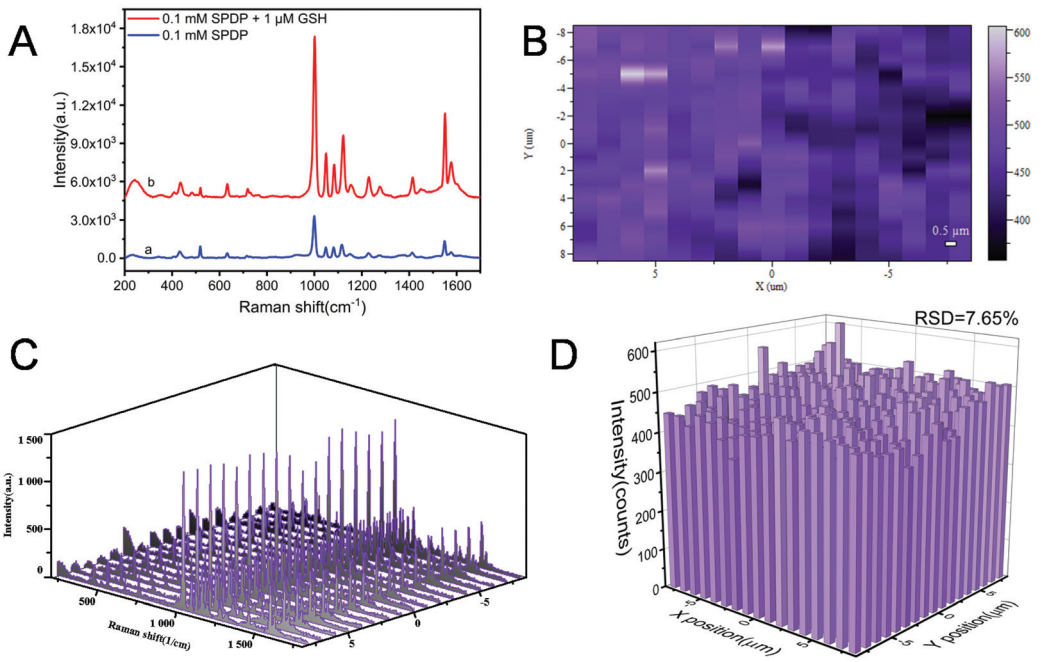

Fig. 4 (A) (a) The SERS spectrum of 0.1 mM SPDP on Ag film@Si and (b) the SERS spectrum of SPDP on the surface of Ag film@Si after mixing and incubating with 1 μM GSH. (B) The heat map of the SERS intensity of SPDP after mixing and incubation with 1 μM GSH; the size of the mapping area was 16 μm × 16 μm. (C) The SERS spectrum of multi-point scanning in the mapping area. (D) The 3D histogram of the SERS intensity corresponding to the mapping area.

SPDP were mixed and incubated for two hours, and the measured SERS spectra are shown in Fig. 5A. It is not difficult to find that when the concentration of GSH gradually increased (Fig. 5A(b–i)), the SERS intensity of SPDP is also increasing (that is, positive correlation) and higher than that of SPDP without GSH (Fig. 5A(a)). Here, the SERS intensity of the characteristic peak located at 1000 cm^{-1} is counted for further analysis. The relative Raman intensity ($I_{SPDP + GSH}/I_{SPDP}$) is obtained through quantitative calculation, and the correlation between it and the concentration of GSH is shown in Fig. 5B. The results show that the relative Raman intensity at 1000 cm^{-1} increases with the increase in GSH concentration. When the concentration is higher than 1 μM, the relative Raman intensity tended to saturate. As can be seen from the vignette of Fig. 5B, when the concentration of GSH is in the range of 10–500 nM, the relative intensity of Raman peak at 1000 cm^{-1} is linearly related to GSH concentration, with an R^2 value of 0.9918. At the same time, Fig. 5C(a) and (b) show the SERS spectrum of the newly prepared Ag film@Si and the substrate after one month of storage for the detection of 1 μM GSH, respectively. It can be seen that the SERS intensity values had little difference, which showed the high stability of the SERS platform. In addition, the interference of adding GSH on the repeatability of the SERS platform was also explored, and the SERS signals on the surface of Ag film@Si of five different batches of silver films were compared. For details, see the ESI

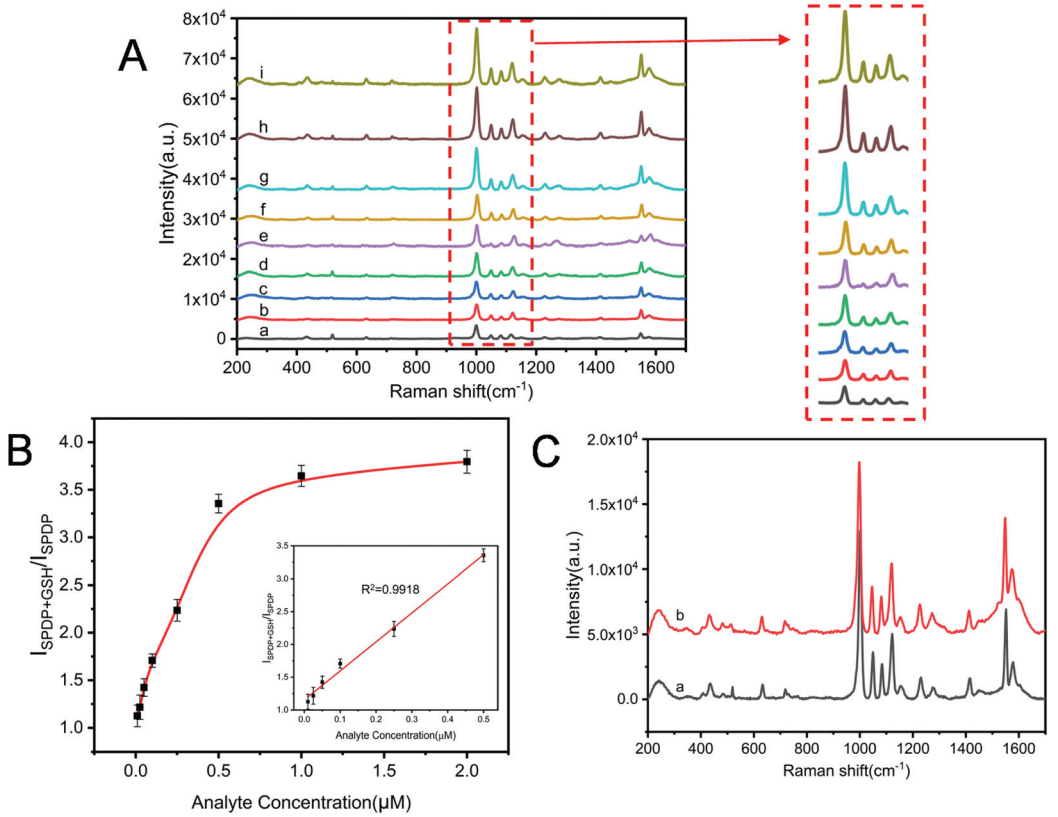

Fig. 5 (A) The SERS spectra of SPDP after incubation with different concentrations of GSH, from a to i are 0 nM, 10 nM, 25 nM, 50 nM, 75 nM, 100 nM, 250 nM, 500 nM, 1000 nM, and 2000 nM. (B) Count of the relative Raman intensity change curve of SPDP at 1000 cm^{-1} after incubation with different concentrations of GSH. (C) The linear plot of the relative Raman intensity at 1000 cm^{-1} in the GSH concentration range of 10 nM to 500 nM. (D) (a) The SERS spectrum of SPDP after incubation with 1 μM GSH and (b) the SERS spectrum of (a) after standing for one month.

(Fig. S1†). An RSD value of 9.64% at 1000 cm^{-1} was calculated quantitatively, indicating that the SERS platform had good repeatability.

In order to further evaluate the SERS detection performance of Ag film@Si for GSH, the above test results were compared with other research results, as shown in ESI Table S1.† The results show that the cost analysis of liquid phase detection is relatively high, the time is longer and the sensitivity is low. The solid phase detection method used in this paper is simple and quick to prepare, easy to transport and carry, and has high sensitivity. The SERS detection method based on Ag film@Si is a reliable, rapid and sensitive method for glutathione evaluation.

Selectivity and practical application of Ag film@Si

Serum is the gelatinous liquid of plasma after fibrinogen has been removed, which provides essential substances for cell growth, such as amino acids, vitamins, and lipids. To explore the selectivity of the indirect detection of GSH by the above SERS platform, the response of other metabolites with similar chemical structures, such as glutamic acid, glycine, histidine, lysine, glucose, homocysteine and cysteine, on the SERS platform was considered. The abovementioned various amino acids (1 μM) were mixed and incubated with SPDP, and SERS determination was carried out according to the same steps. All test conditions remain the same as before. Fig. 6A(b–h) shows the SERS signals of SPDP after adding seven different amino acids, respectively. The original SERS signals of SPDP are shown in Fig. 6A(i). Fig. 6A(a) shows the SERS spectrum when 1 μM GSH was added. Compared to the SERS spectra of other amino acids, the intensity is significantly greater. In order to quantitatively evaluate the interference degree of other amino acids on the SERS platform, the SERS intensity value with the characteristic peak located at 1000 cm^{-1} was statistically analyzed. The relative intensity obtained is shown in the histogram of Fig. 6B. With the addition of GSH, the relative Raman intensity of SPDP expanded by 3.48 times, which is higher than the relative Raman intensity of SPDP caused by other similar amino acids. Therefore, the SERS platform can realize selective detection of GSH.

In order to explore the possibility of practical applications of this method, real serum samples were selected as the external environment for GSH. Normal human serum was pretreated first and then 0.1 mM SPDP and 1 μM GSH were prepared with serum as the solvent. Then the two were mixed and incubated for two hours, and SERS detection was carried out according to the above method. Fig. 7A(a) shows the SERS spectrum of SPDP in serum, Fig. 7A(b) shows the SERS spectrum of 0.1 mM SPDP in serum containing 1 μM GSH, Fig. 7A

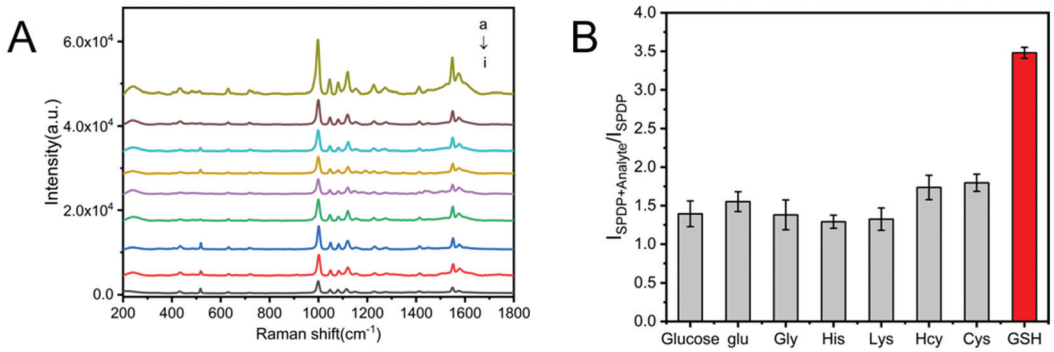

Fig. 6 (A) Similar amino acid (from a to h are GSH, Cys, Hcy, Lys, His, Gly, glu, and glucose) SERS spectra of SPDP after incubation and (i) the SERS spectra of SPDP. (B) The relative Raman intensity histogram of SPDP at 1000 cm^{-1} after incubation with similar amino acids.

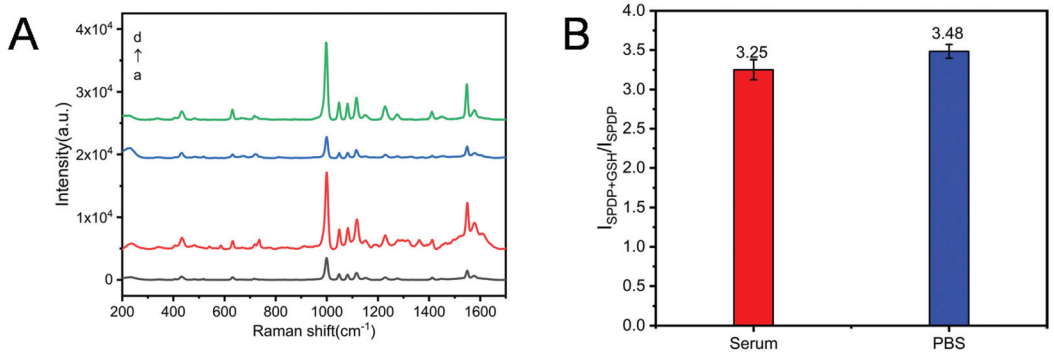

Fig. 7 (A) (a) The SERS spectrum of 0.1 mM SPDP in serum, (b) the SERS spectrum of 0.1 mM SPDP in serum containing 1 μM GSH, (c) the SERS spectrum of 0.1 mM SPDP diluted with PBS, and (d) the SERS spectrum of 1 μM GSH dissolved in PBS and 0.1 mM SPDP mixed and incubated. (B) The histogram of the relative Raman intensity of SPDP at 1000 cm^{-1}.

(c) shows the SERS spectrum of 0.1 mM SPDP diluted with PBS, and Fig. 7A(d) shows the SERS spectrum of 1 μM GSH dissolved in PBS and 0.1 mM SPDP after mixed incubation. It is obvious that there is a little noise in the spectrum of SPDP in the serum, but the spectral intensity has not changed much, and the characteristic Raman peak position has not changed. In order to quantitatively evaluate the interference degree of the external environment, the relative Raman intensity of the statistical characteristic peak at 1000 cm^{-1} is plotted in a histogram as shown in Fig. 7B. The relative Raman intensity in serum at 1000 cm^{-1} is 3.25, which is slightly lower than that in PBS. Thus, it can be seen that the SERS sensing platform designed by this scheme has the possibility of practical applications, which provides a basis for the quantitative detection of glutathione. In addition, the results were compared with those of DTNB colorimetry, as detailed in ESI and Fig. S3.† After 90 min of reaction, the absorbance value of the serum containing 1 μM GSH exceeds the maximum value of the standard value. At this time, the DTNB colorimetric method may have failed. The SERS detection method based on Ag film@Si can avoid the possible data deviation caused by enzyme activity damage and has high sensitivity. Therefore, when the external environment becomes more complicated, the SERS platform can provide a detection possibility for actual detection.

Conclusions

In this paper, a novel SERS sensing platform based on simply synthesized and self-assembled Ag film@Si is proposed for the detection of GSH with high sensitivity and selectivity. With the aid of the oil/water/oil three-phase system, silver nanofilms were self-assembled and finally deposited on a silicon wafer. The heterobifunctional crosslinking agent SPDP, which contains pyridine rings and disulfide bonds, was involved in the exchange reaction between the sulfhydryl groups and disulfide bonds. With the addition of GSH, the breakage of disulfide bonds was promoted, thereby enhancing the SERS signal of SPDP. By detecting the change in the SERS signal of SPDP, GSH can be detected sensitively. The minimum detection sensitivity of GSH is 10 nM, and a good linear relationship of GSH is found in the range of 10–500 nM. Simultaneously, Ag film@Si also shows good uniformity and the relative standard deviation of the SERS intensity is about 7.65%. When other similar amino acid interferences were explored, the SERS platform could realize the selective detection of GSH. Considering the clinical detection of GSH levels when the external environment is serum or other more complex environments, the DTNB colorimetry reached its limit at 1 μM GSH. Moreover, this method is susceptible to enzyme activity damage and has

poor stability. Therefore, the method proposed in this paper has the prospect of highly sensitive and quantitative detection of GSH.

Conflicts of interest

There are no conflicts to declare.

Acknowledgements

This work was supported by the National Natural Science Foundation of China under Grant No. 51972292 and the Fundamental Research Funds for the Provincial Universities of Zhejiang under Grant No. 2020YW09.

References

1 M. L. Reniere, A. T. Whiteley, K. L. Hamilton, S. M. John, P. Lauer, R. G. Brennan and D. A. Portnoy, *Nature*, 2015, **517**, 170–173.
2 C. R. Corso and A. Acco, *Crit. Rev. Oncol. Hematol.*, 2018, **128**, 43–57.
3 Z. Liu, X. Zhou, Y. Miao, Y. Hu, N. Kwon, X. Wu and J. Yoon, *Angew. Chem., Int. Ed.*, 2017, **56**, 5812–5816.
4 G. Teskey, R. Abrahem, R. Cao, K. Gyurjian, H. Islamoglu, M. Lucero, A. Martinez, E. Paredes, O. Salaiz, B. Robinson and V. Venketaraman, *Adv. Clin. Chem.*, 2018, **87**, 141–159.
5 P. Diaz-Vivancos, A. de Simone, G. Kiddle and C. H. Foyer, *Free Radicals Biol. Med.*, 2015, **89**, 1154–1164.
6 L. E. Hernandez, J. Sobrino-Plata, M. B. Montero-Palmero, S. Carrasco-Gil, M. L. Flores-Caceres, C. Ortega-Villasante and C. Escobar, *J. Exp. Bot.*, 2015, **66**, 2901–2911.
7 S. P. Hadipour Moghaddam, M. Yazdimamaghani and H. Ghandehari, *J. Controlled Release*, 2018, **282**, 62–75.
8 S. Lee, J. Li, X. Zhou, J. Yin and J. Yoon, *Coord. Chem. Rev.*, 2018, **366**, 29–68.
9 S. Panday, R. Talreja and M. Kavdia, *Microvasc. Res.*, 2020, **131**, 104010–104025.
10 A. Polonikov, *ACS Infect. Dis.*, 2020, **6**, 1558–1562.
11 C. Wei, X. Liu, Y. Gao, Y. Wu, X. Guo, Y. Ying, Y. Wen and H. Yang, *Anal. Chem.*, 2018, **90**, 11333–11339.
12 K. Umezawa, M. Yoshida, M. Kamiya, T. Yamasoba and Y. Urano, *Nat. Chem.*, 2017, **9**, 279–286.
13 C. Zhan, G. Zhang and D. Zhang, *ACS Appl. Mater. Interfaces*, 2018, **10**, 12141–12149.
14 A. Tsiasioti, I. Iakovidou, C. K. Zacharis and P. D. Tzanavaras, *Spectrochim. Acta, Part A*, 2020, **229**, 117963–117968.
15 F. Yan, Z. Sun, J. Xu, H. Li and Y. Zhang, *Mikrochim. Acta*, 2020, **187**, 344–352.
16 J. Escobar, A. Sanchez-Illana, J. Kuligowski, I. Torres-Cuevas, R. Solberg, H. T. Garberg, M. U. Huun, O. D. Saugstad, M. Vento and C. Chafer-Pericas, *J. Pharm. Biomed. Anal.*, 2016, **123**, 104–112.
17 L. Wei, Y. Song, P. Liu and X. Kang, *Mikrochim. Acta*, 2018, **185**, 321–328.
18 Y. Wang, L. Jiang, L. Chu, W. Liu, S. Wu, Y. Wu, X. He and K. Wang, *Biosens. Bioelectron.*, 2017, **87**, 459–465.
19 Z. Wang, P. Han, X. Mao, Y. Yin and Y. Cao, *Sens. Actuators, B*, 2017, **238**, 325–330.
20 Y. Xianyu, Y. Xie, N. Wang, Z. Wang and X. Jiang, *Small*, 2015, **11**, 5510–5514.
21 V. Kumar, D. Bano, D. K. Singh, S. Mohan, V. K. Singh and S. H. Hasan, *ACS Sustainable Chem. Eng.*, 2018, **6**, 7662–7675.
22 Z. Chen, L. Chen, L. Lin, Y. Wu and F. Fu, *ACS Sens.*, 2018, **3**, 2145–2151.
23 X. Ji, W. Wang, X. Li, Y. Chen and C. Ding, *Talanta*, 2016, **150**, 666–670.
24 Á. Sánchez-Illana, F. Mayr, D. Cuesta-García, J. D. Piñeiro-Ramos, A. Cantarero, M. D. L. Guardia, M. Vento, B. Lendl, G. Quintás and J. Kuligowski, *Anal. Chem.*, 2018, **90**, 9093–9100.
25 Y. Liu, J. Lu, Y. Tao, N. Li, M. Yang and J. Shao, *Anal. Chem.*, 2020, **92**, 9566–9573.
26 J. Langer, D. Jimenez de Aberasturi, J. Aizpurua, R. A. Alvarez-Puebla, B. Auguie, J. J. Baumberg, G. C. Bazan, S. E. J. Bell, A. Boisen, A. G. Brolo, J. Choo, D. Cialla-May, V. Deckert, L. Fabris, K. Faulds, F. J. Garcia de Abajo, R. Goodacre, D. Graham, A. J. Haes, C. L. Haynes, C. Huck, T. Itoh, M. Kall, J. Kneipp, N. A. Kotov, H. Kuang, E. C. Le Ru, H. K. Lee, J. F. Li, X. Y. Ling, S. A. Maier, T. Mayerhofer, M. Moskovits, K. Murakoshi, J. M. Nam, S. Nie, Y. Ozaki, I. Pastoriza-Santos, J. Perez-Juste, J. Popp, A. Pucci, S. Reich, B. Ren, G. C. Schatz, T. Shegai, S. Schlucker, L. L. Tay, K. G. Thomas, Z. Q. Tian, R. P. Van Duyne, T. Vo-Dinh, Y. Wang, K. A. Willets, C. Xu, H. Xu, Y. Xu, Y. S. Yamamoto, B. Zhao and L. M. Liz-Marzan, *ACS Nano*, 2020, **14**, 28–117.
27 J. Lee, Q. Zhang, S. Park, A. Choe, Z. Fan and H. Ko, *ACS Appl. Mater. Interfaces*, 2016, **8**, 634–642.
28 Y. Wang, Y. Wang, W. Wang, K. Sun and L. Chen, *ACS Appl. Mater. Interfaces*, 2016, **8**, 28105–28115.
29 E. C. Le Ru and P. G. Etchegoin, *Annu. Rev. Phys. Chem.*, 2012, **63**, 65–87.
30 Y. Wang, B. Yan and L. Chen, *Chem. Rev.*, 2013, **113**, 1391–1428.
31 J. Kuligowski, M. R. El-Zahry, A. Sanchez-Illana, G. Quintas, M. Vento and B. Lendl, *Analyst*, 2016, **141**, 2165–2174.
32 W. Wang, L. Zhang, L. Li and Y. Tian, *Anal. Chem.*, 2016, **88**, 9518–9523.
33 X. Lin, W. L. Hasi, S. Q. Han, X. T. Lou, D. Y. Lin and Z. W. Lu, *Phys. Chem. Chem. Phys.*, 2015, **17**, 31324–31331.
34 H. Zhao, W. Hasi, N. Li, X. Sha and S. Han, *J. Raman Spectrosc.*, 2019, **50**, 1679–1690.
35 X. Lin, S. Lin, Y. Liu, M. Gao, H. Zhao, B. Liu, W. Hasi and L. Wang, *Langmuir*, 2018, **34**, 6077–6084.
36 Y. Qin, X. Ji, J. Jing, H. Liu, H. Wu and W. Yang, *Colloids Surf., A*, 2010, **372**, 172–176.

37 X. Lin, G. Fang, Y. Liu, Y. He, L. Wang and B. Dong, *J. Phys. Chem. Lett.*, 2020, **11**, 3573–3581.
38 W. Zhou, B. C. Yin and B. C. Ye, *Biosens. Bioelectron.*, 2017, **87**, 187–194.
39 B. Pal, P. K. Bajpai, J. Sengupta and V. Singh, *J. Raman Spectrosc.*, 1997, 323–329.
40 H. Liao and J. H. Hafner, *Chem. Mater.*, 2005, **17**, 4636–4641.
41 A. Pallaoro, M. R. Hoonejani, G. B. Braun, C. Meinhart and M. Moskovits, *J. Nanophotonics*, 2013, **7**, 073092–073102.
42 E. Dumont, C. De Bleye, M. Haouchine, L. Coic, P. Y. Sacre, P. Hubert and E. Ziemons, *Spectrochim. Acta, Part A*, 2020, **233**, 118180–118188.
43 J. Carlsson, H. Drevin and R. Axen, *Biochem. J.*, 1978, **173**, 723–737.
44 S. Ferretti, S. Paynter, D. A. Russell, K. E. Sapsford and D. J. Richardson, *Trends Anal. Chem.*, 2000, **19**, 530–540.
45 J. Li, L. Chen, T. Lou and Y. Wang, *ACS Appl. Mater. Interfaces*, 2011, **3**, 3936–3941.
46 A. Selvarajan, *Proc. - Indian Acad. Sci., Sect. A*, 1966, **64**, 44–50.